JCTC Journal of Chemical Theory and Computation

Article

pubs.acs.org/JCTC

# Ground- and Excited-State Geometry Optimization of Small Organic Molecules with Quantum Monte Carlo

Riccardo Guareschi and Claudia Filippi*

MESA+ Institute for Nanotechnology, University of Twente, P.O. Box 217, 7500 AE Enschede, The Netherlands

Supporting Information

**ABSTRACT:** We present a comparative study of the geometry optimization in the gas phase of acrolein, acetone, methylenecyclopropene, and the propenoic acid anion with special emphasis on their excited-state structures, using quantum Monte Carlo (QMC), multireference perturbation theory (CASPT2 and NEVPT2), second-order approximate coupled cluster (CC2), and time-dependent density functional theory (TDDFT). We find that, for all molecules, the geometries optimized with QMC in its simplest variational (VMC) flavor are in very good agreement with the perturbation results both in the ground and the excited states of either $n \rightarrow \pi^*$ or $\pi \rightarrow \pi^*$ character. Furthermore, the quality of the QMC structures is superior to those obtained with the CC2 method, which overestimates the CO bond in all $n \rightarrow \pi^*$ excitations, or to the symmetry-adapted-cluster configuration interaction (SAC−CI) approach, which gives a poorer description of the CC bonds in the excited states. Finally, the spread in the TDDFT structures obtained with several current exchange-correlation functionals is large and does not reveal a clear relation between the defining features of the functionals and the quality of the optimized structures. In summary, our findings demonstrate the good performance of QMC in optimizing the geometries of these molecules, also in cases where other correlated or TDDFT approaches are inaccurate, and indicate that the method represents a robust reference approach for future structural studies also of larger systems.

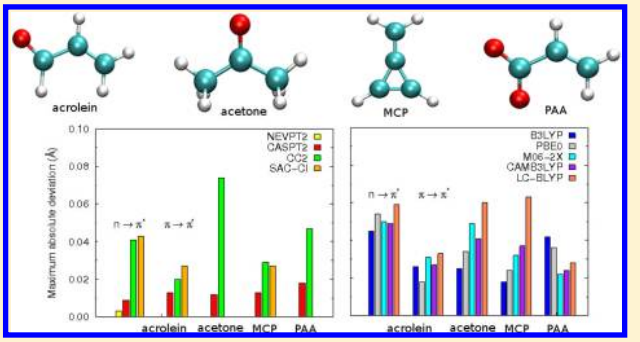


## 1. INTRODUCTION

The optimization of ground- and excited-state structures of molecular systems is an area of fundamental importance in the application of quantum chemical methods. While it is possible to choose among a variety of first-principle approaches, these often display different performances as regards the computational cost or the accuracy of the resulting structures, especially if one considers geometrical relaxation in an electronically excited state.

Time-dependent density functional theory (TDDFT) is the most efficient approach for the computation of excited states of large molecules[1−3] but relies in practice on the choice of an approximate exchange-correlation functional, which may severely limit its accuracy, in particular in describing excitations characterized by charge transfer or multireference character.[4,5] Therefore, significant research effort has been devoted to develop novel functionals, the long-range corrected being just one example,[6−13] and to benchmark the performance of the numerous available approximations.[14−25] Benchmarking has mostly focused on the quality of the vertical excitation energies[16−18,21] but several studies have recently attempted to also establish the performance of TDDFT in describing the optimal excited-state structures and fluorescence[14,20,23,24] also with the inclusion of a solvent via the polarizable continuum model.[15,19,22,25] While these investigations concur on the fact that the spread of TDDFT geometries obtained with different exchange-correlation functionals can be rather large, the assessment of the relative accuracy of these structures is hindered by the corresponding spread of reference geometries obtained at a higher level of theory.

The complete-active-space second-order perturbation theory (CASPT2), symmetry-adapted-cluster configuration interaction (SAC−CI), and second-order approximate coupled-cluster (CC2) have been adopted as reference in different TDDFT studies[19,23,25] but these approaches may yield significantly different equilibrium geometries in the excited state of some particular molecule. For instance, CC2 generally overestimates the CO bond lengths in the $n \rightarrow \pi^*$ excited states[25,26] and the selection of this reference method can clearly introduce a bias in the evaluation of the quality of a TDDFT geometrical optimization.

Quantum Monte Carlo (QMC) methods represent an alternative class of highly correlated approaches, which solve the Schrödinger equation by stochastic means, enabling the use of accurate and compact many-body wave functions with an explicit dependence on the interparticle distances.[27−29] While the most common variational (VMC) and diffusion (DMC) Monte Carlo variants have been routinely employed for the study of ground-state properties of molecules and solids, their use for the investigation of excited states mainly dates to the past few

Received: October 8, 2013

   dx.doi.org/10.1021/ct400876y | J. Chem. Theory Comput. XXXX, XXX, XXX−XXX

years[30−41] and has been primarily restricted to the computation of vertical excitation energies. Importantly, these approaches have been shown to yield excitation energies for several prototypical photosensitive molecules[36−41] in good agreement with multireference perturbation approaches as CASPT2 in its most recent IPEA formulation[42] and the *n*-electron valence perturbation theory (NEVPT2).[43] Geometry optimization[37,44−47] is also possible within QMC thanks to recent methodological advances, in particular, the robust optimization of wave functions within VMC in a state-specific[48] and state-average[36] fashion, and the computation of interatomic forces with a finite-variance estimator[44] and efficient analytic expressions.[45] To date, the only attempt to optimize the geometry of a nontrivial excited state via QMC gradients remains however our work on retinal chromophore models.[37]

In this paper, we present a detailed QMC study of the excited-state structures (stationary points and global minima) obtained for a set of small organic molecules in the gas phase (*s*-cis and *s*-trans acrolein, acetone, methylenecyclopropene, and the propenoic acid anion) often used to assess the accuracy of TDDFT or other approaches. The aim of this paper is 2-fold. Since QMC has not been often used to optimize the geometry of excited states, we want to demonstrate here the good quality of VMC geometries as well as offer a comparison with other popular methods often used in benchmark studies. To this purpose, we revisit the optimization of the structures within CASPT2 (and within NEVPT2 for some of these molecules), paying particular attention to the choice of the active space used in the reference wave function. This can, in fact, significantly affect the resulting optimal geometry as in the case of the propenoic acid anion, where we obtain a different equilibrium structure than in previous CASPT2 studies.[49] In addition to these perturbation approaches, we also compare our QMC results with the structures we obtain with CC2 and a variety of present-day TDDFT functionals, as well as with SAC−CI results available in the literature.[50] Our comparative study demonstrates that the use of VMC interatomic gradients in combination with fully optimized wave functions yields very accurate excited-state structures and that VMC represents a robust reference theory for future benchmark studies.

In Section 2, we present the computational details and, in Section 3, discuss various methodological aspects regarding the wave functions and the computation of interatomic gradients in QMC. In Section 4, we present a detailed analysis of our results, and we conclude in Section 5.

## 2. COMPUTATIONAL DETAILS

We perform the TDDFT calculations with the Gaussian09 program[51] and employ a set of exchange-correlation functionals that are representative of different classes of approximations. In particular, we use BLYP[52,53] as local functional with no Hartree−Fock (HF) exchange, B3LYP,[54,55] PBE0,[56−58] M06,[59] and M06-2X[59] as global hybrids with a fixed amount of HF exchange, and CAM-B3LYP,[6] and LC-BLYP[7] for the long-range corrected functionals with a variable percentage of HF exchange, which depends on the interelectronic distance.

We carry out the CC2[60−63] calculations with the CFOUR code[64] and use the MOLCAS 7.2 suite of programs[65] for the CASPT2[66,67] calculations, where we always employ the default zero-order IPEA Hamiltonian.[42] The strongly contracted (SC) NEVPT2[43,68,69] calculations are performed with the ORCA 2.8 code.[70] With this code, one can exploit symmetry in the single-point calculations but not in the geometry optimization with numerical gradients at the NEVPT2 level. Furthermore, ORCA employs the weighted average of the interatomic gradients to optimize with NEVPT2 the structure of an excited state resulting from a state-average calculation. Therefore, we only employ NEVPT2 to optimize the geometry in the ground state and in the lowest-energy state with a different symmetry than the ground state using a fictitious state-average calculation over two roots with (0,1) weights. This procedure is, however, only successful for the $n \rightarrow \pi^*$ excited state of acrolein.

The program package CHAMP is used for the QMC calculations.[71] We employ scalar-relativistic energy-consistent Hartree−Fock pseudopotentials[72,73] and obtain the starting determinantal component of the Jastrow−Slater wave function in complete-active-space self-consistent field (CASSCF) calculations performed with the program GAMESS(US).[74] The CAS expansions are then expressed on the CASSCF natural orbitals and all configuration state functions are retained in the QMC studies. Only for the propenoic acid anion, the expansion is truncated with a threshold of 0.05 on the CSF coefficients for subsequent use in the QMC calculations. All parameters in the QMC wave functions are optimized in variational Monte Carlo using the linear method[48] and its extension for state-average calculations.[36] Further details on the QMC calculations are given in the Methods section.

The basis set dependence of the geometrical parameters is studied at the TDDFT, CASPT2, NEVPT2, and CC2 level using the Dunning's correlation consistent cc-pVXZ and aug-cc-pVXZ basis sets.[75−78] In the QMC calculations, we use the Gaussian basis sets[72] specifically constructed for our pseudopotentials. In particular, we employ the cc-pVDZ and cc-pVTZ basis sets and the corresponding basis augmented with diffuse functions[79] on the heavy atoms. We also use the cc-pVTZ′ basis set which consist of the cc-pVTZ for the heavy atoms combined with the cc-pVDZ for hydrogen. We show below that the geometrical parameters computed with the TDDFT, CC2, and perturbation methods are well converged with the cc-pVTZ basis set and, within QMC, with the cc-pVTZ′ basis.

## 3. METHODS

QMC methods provide an accurate and balanced description of dynamical and static electronic correlation in molecular systems for the computation of ground- and excited-state properties. The most commonly used QMC wave functions are of the so-called Jastrow−Slater type, namely, a linear combination of spin-adapted configuration state functions (CSFs) multiplied by a Jastrow correlation factor, $\mathcal{J}$:

$$\Psi_I = \mathcal{J} \sum_{i=1}^{N_{\mathrm{CSF}}} c_i C_i \tag{1}$$

where $c_i$ are the expansion coefficients of the CSFs, $C_i$, for the state of interest, *I*. The Jastrow factor depends explicitly on the interparticle distances and we consider here different Jastrow forms either including only two-body interactions ($\mathcal{J}_{2-\mathrm{body}}$) to account for electron−nuclear and electron−electron correlations, or also also three-body terms to describe electron−electron-nuclear correlations ($\mathcal{J}_{3-\mathrm{body}}$).[80] Different Jastrow factors are used to describe different atom types.

The linear coefficients, the orbitals, and the Jastrow parameters are optimized by energy minimization within VMC in a state-specific[48] or state-average[36] fashion. If we are interested in the lowest state of a given symmetry, we simply minimize the


dx.doi.org/10.1021/ct400876y | J. Chem. Theory Comput. XXXX, XXX, XXX−XXX

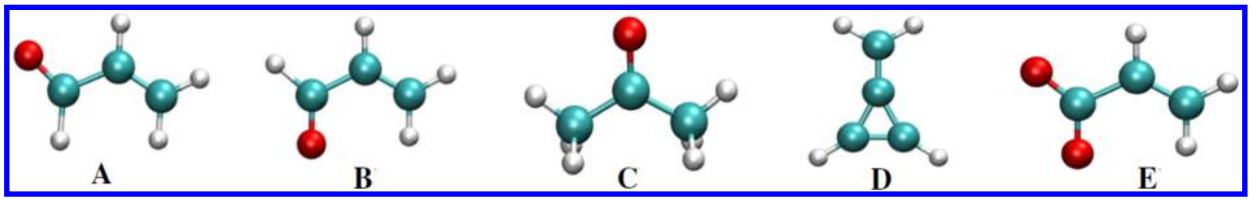


**Figure 1.** The molecules considered in this work: (A) *s*-trans and (B) *s*-cis acrolein, (C) acetone, (D) methylenecyclopropene (MCP), and (E) the propenoic acid anion (PAA).

corresponding variational energy with respect to the wave function parameters. In the case of a not-trivial excited state with lower-energy states of the same symmetry, we minimize the weighted-averaged energy over the states under consideration:

$$E_{\mathrm{SA}} = \sum_{I}^{\mathrm{Nstates}} w_I \frac{\langle \Psi_I | \mathcal{H} | \Psi_I \rangle}{\langle \Psi_I | \Psi_I \rangle} \tag{2}$$

where the weights sum to one. The wave functions $\Psi_I$ of the different states share a common set of single-particle orbitals and a common Jastrow factor but depend on their individual linear coefficients $c_i^I$, which are determined to ensure orthogonality between the states. At convergence, the averaged energy is stationary with respect to all parameter variations subject to the orthogonality constraint, while the energies of the individual states are stationary with respect to variations of the linear coefficients but not with respect to variations of the orbital or Jastrow parameters. In the case of multiple states, the expectation values of the quantities needed for the optimization of the parameters are computed in a single VMC run by sampling the square of a guiding wave function, $\Psi_g^2$, which is here chosen equal to $\sum_I |\Psi_I|^2$.

The VMC geometry optimizations are performed in Z-matrix coordinates with the use of numerical gradients of the energy with respect to the atomic coordinates. The interatomic forces at a reference geometry are computed in a correlated sampling VMC calculation,[81] where a set of secondary geometries is generated through forward and backward displacements of 0.001 au in the bond lengths and 0.01° in the bond and dihedral angles. To obtain stable estimates of the gradients in the correlated sampling runs, we follow ref 44 and sample a distribution which is finite at the nodes. The procedure followed here is described in greater detail in our previous work on structural optimization in VMC[37] and can be summarized in the following steps: (i) The Jastrow parameters, linear coefficients, and the orbitals of the starting wave function are optimized in energy minimization at the initial geometry; (ii) the energy gradients are computed in a correlated sampling VMC calculation; (iii) the geometry is updated following the descendant direction of the energy gradient in an approximate Newton−Raphson method which uses the diagonal elements of the Hessian; (iv) at the new geometry, the wave function is optimized starting form the optimal wave function at the previous step, recentered at the new geometry. The procedure is iterated until convergence, namely, until the forces are smaller than 0.001−0.003 hartree/Bohr for the bond lengths and 0.0001 hartree/deg for the bond angles. As starting geometries in the ground-state optimizations, we usually employ a DFT structure and, in the excited-state relaxation, an excited-state geometry obtained with another correlated theory. For the more problematic case of the $\pi \rightarrow \pi^*$ state of planar acrolein, we test the use of the ground-state VMC geometry as initial guess and obtain the same final configuration. All VMC structural optimizations converge with less than 10 iterations.

Due to the stochastic nature of VMC, it is not possible to identify a particular geometry as the minimum one. Therefore, after convergence, we perform 5−10 more iterations and obtain the final structure by averaging the internal coordinates over these additional steps. For the geometry optimization of an excited state which is not the lowest in its symmetry class, the wave function parameters are optimized in a state-average manner as described above, but the forces are computed for the root of interest. We note that analytic calculation of VMC forces is possible to reduce the computational cost for systems larger than the ones studied here.[45] Finally, approximate DMC forces[81] could also be employed but their use in combination with fully optimized wave functions does not seem to improve the VMC estimates,[37,47] while being significantly more expensive.

## 4. RESULTS

The molecules investigated here are the *s*-trans and *s*-cis acrolein, acetone, methylenecyclopropene (MCP), and the propenoic acid anion (PAA), which are shown in Figure 1. This set of representative molecules has often been chosen in the literature to study the performance of quantum chemical methods in determining optimal excited-state structures.[19,25,49,50,82−89] We consider the structural optimization in the ground state of all molecules, in the $n \rightarrow \pi^*$ state of acrolein, acetone, and PAA, and in the $\pi \rightarrow \pi^*$ state of acrolein and MCP.

The geometries of these molecules are optimized with different symmetry constraints in their ground and low-lying singlet excited states as detailed in Table 1. When planarity is imposed in the excited state, the optimal structures do not correspond to a minimum in the case of acrolein and MCP in the

**Table 1. Symmetries Imposed in the Structural Optimization of the Ground and Low-Lying Excited States of the Molecules**[a]

| molecule | symmetry | state | excitation |
|---|---|---|---|
| *s*-trans acrolein | $C_s$ planar | $1^1A'$ | GS |
| | | $1^1A''$ | $n \rightarrow \pi^*$ |
| | | $2^1A'$ | $\pi \rightarrow \pi^*$ |
| | $C_s$ twisted | $1^1A''$ | GS |
| *s*-cis acrolein | $C_s$ planar | $1^1A'$ | GS |
| | | $1^1A''$ | $n \rightarrow \pi^*$ |
| acetone | $C_{2v}$ planar | $1^1A_1$ | GS |
| | | $1^1A_2$ | $n \rightarrow \pi^*$ |
| | $C_s$ bended | $1^1A''$ | $n \rightarrow \pi^*$ |
| MCP | $C_{2v}$ planar | $1^1A_1$ | GS |
| | | $1^1B_2$ | $\pi \rightarrow \pi^*$ |
| PAA | $C_s$ planar | $1^1A'$ | GS |
| | | $1^1A''$ | $n \rightarrow \pi^*$ |

[a]The symmetry of the state and the nature of the excitation are also reported. We denote with GS the lowest-energy state for the given geometry.


dx.doi.org/10.1021/ct400876y | J. Chem. Theory Comput. XXXX, XXX, XXX−XXX

$\pi \rightarrow \pi^*$ state, and of acetone in the $n \rightarrow \pi^*$ state. For acetone, we also determine the minimum geometry for the $n \rightarrow \pi^*$ state, allowing the pyramidalization of the central C atom, which leads to a symmetry reduction from $C_{2v}$ to $C_s$. The out-of-plane optimization is also performed for *s*-trans acrolein in the $\pi \rightarrow \pi^*$ excited state, where a twisting around the terminal C−$CH_2$ bond is expected to bring the system to the minimum energy geometry with a diradical ground state.

For these states and molecules, we compute the optimal geometries within VMC, CC2, CASPT2, and NEVPT2. We assess the relative performance of these highly correlated methods and compare our results to the geometries obtained with different approximate exchange-correlation functionals within TDDFT. Before presenting the results of our geometry optimizations, we first discuss the dependence of the geometrical parameters obtained with the various methods on the choice of basis set and, in the VMC calculations, on the sophistication of the Jastrow factor. To illustrate the dependence of the methods on these computational ingredients, we focus on for *s*-trans acrolein in the ground and the $n \rightarrow \pi^*$ excited state and report the same study for the other systems in the Supporting Information.

**4.1. Geometry Dependence on Basis Set.** For *s*-trans acrolein, we employ the cc-pVXZ and aug-cc-pVXZ series to investigate the basis set dependence of the optimal structures computed at the CASPT2, NEVPT2, CC2, and TDDFT level in the ground and the lowest $n \rightarrow \pi^*$ excited state.

We report the CASPT2 ground- and excited-state geometries obtained with the cc-pVXZ basis sets in Table 2. The

**Table 2. CASPT2 Bond Lengths (Å) and Angles (deg) of *s*-Trans Acrolein in the Ground ($1^1A'$) and $n \rightarrow \pi^*$ Excited ($1^1A''$) States Computed with the cc-pVXZ Basis Sets**

| CASPT2 | cc-pVDZ | cc-pVTZ | cc-pVQZ |
|---|---|---|---|
| | $1^1A'$ | | |
| C═O | 1.220 | 1.214 | 1.211 |
| C−C | 1.482 | 1.470 | 1.468 |
| C═C | 1.352 | 1.339 | 1.337 |
| $\theta$(C−C−C) | 120.78 | 120.36 | 120.25 |
| $\theta$(C−C−O) | 124.02 | 124.16 | 122.67 |
| | $1^1A''$ | | |
| C═O | 1.342 | 1.336 | 1.332 |
| C−C | 1.388 | 1.377 | 1.375 |
| C═C | 1.406 | 1.392 | 1.389 |
| $\theta$(C−C−C) | 123.36 | 123.26 | 123.26 |
| $\theta$(C−C−O) | 124.93 | 1124.54 | 124.36 |

enlargement of the basis set from double to quadruple $\zeta$ produces a slight shortening of the bond lengths, which are well converged when the cc-pVTZ basis is employed. The cc-pVDZ bond lengths differ from the cc-pVQZ values by at most 0.017 Å and the use of cc-pVTZ improves the agreement to better than 0.005 Å. The effect of the augmentation is tested only for the excited state where it might be expected to have an effect. As shown in Figure 2, we find instead that the aug-cc-pVXZ series does not performs better than the cc-pVXZ sets since, for the smallest double $\zeta$ basis, it leads to geometries further away from the converged values. As shown in Tables 3 and 4, the cc-pVTZ basis leads to well converged geometries in the ground and excited states also at the NEVPT2 and CC2 level. Also, for these methods, we observe a slower convergence if the geometries are optimized with the aug-cc-pVXZ basis sets, especially for the C−O bond length in the excited state (see Supporting Information).

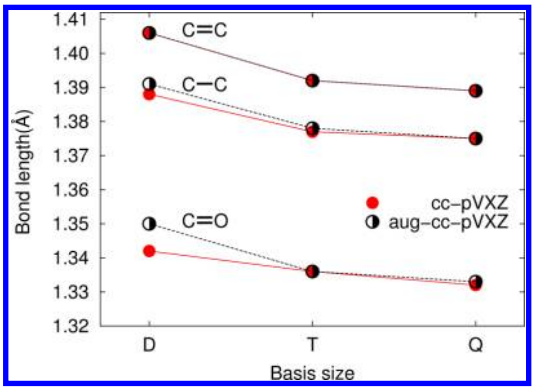


**Figure 2.** Convergence of the bond lengths (Å) of *s*-trans acrolein in the $n \rightarrow \pi^*$ excited state computed at the CASPT2 level with the cc-pVXZ basis sets.

**Table 3. NEVPT2 Bond Lengths (Å) and Angles (deg) of *s*-Trans Acrolein in the Ground ($1^1A'$) and $n \rightarrow \pi^*$ Excited ($1^1A''$) States Computed with Different Basis Sets**

| NEVPT2 | cc-pVDZ | cc-pVTZ | cc-pVQZ |
|---|---|---|---|
| | $1^1A'$ | | |
| C═O | 1.219 | 1.210 | 1.209 |
| C−C | 1.479 | 1.462 | 1.458 |
| C═C | 1.350 | 1.333 | 1.329 |
| $\theta$(C−C−C) | 120.72 | 120.33 | 119.66 |
| $\theta$(C−C−O) | 124.19 | 124.45 | 123.90 |
| | $1^1A''$ | | |
| C═O | 1.339 | 1.328 | 1.326 |
| C−C | 1.387 | 1.371 | 1.371 |
| C═C | 1.403 | 1.385 | 1.383 |
| $\theta$(C−C−C) | 123.40 | 123.37 | 123.42 |
| $\theta$(C−C−O | 125.00 | 124.79 | 124.39 |

**Table 4. CC2 Bond Lengths (Å) and Angles (deg) of *s*-Trans Acrolein in the Ground ($1^1A'$) and $n \rightarrow \pi^*$ Excited ($1^1A''$) States Computed with Different Basis Sets**

| CC2 | cc-pVDZ | cc-pVTZ | cc-pVQZ |
|---|---|---|---|
| | $1^1A'$ | | |
| C═O | 1.229 | 1.221 | 1.220 |
| C−C | 1.481 | 1.463 | 1.462 |
| C═C | 1.353 | 1.336 | 1.335 |
| $\theta$(C−C−C) | 120.28 | 120.00 | 119.97 |
| $\theta$(C−C−O) | 124.45 | 124.56 | 124.38 |
| | $1^1A''$ | | |
| C═O | 1.369 | 1.368 | 1.371 |
| C−C | 1.391 | 1.370 | 1.369 |
| C═C | 1.398 | 1.383 | 1.382 |
| $\theta$(C−C−C) | 122.20 | 122.14 | 122.15 |
| $\theta$(C−C−O) | 127.83 | 127.15 | 126.67 |

To investigate the basis set dependence of the TDDFT geometries, we select the CAM-B3LYP functional since the convergence is rather similar for the different functionals. The dependence of the bond lengths in the excited state are shown in Figure 3 and is rather similar to the one observed for the perturbation and CC2 methods, with bond lengths which are well converged when the cc-pVTZ basis is employed. The aug-cc-pVXZ series yields practically equivalent results to the cc-pVXZ sets.


dx.doi.org/10.1021/ct400876y | J. Chem. Theory Comput. XXXX, XXX, XXX−XXX

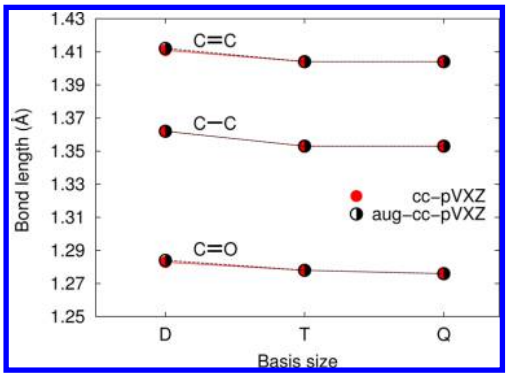


**Figure 3.** Convergence of the bond lengths (Å) of *s*-trans acrolein in the $n \rightarrow \pi^*$ excited state computed within TDDFT/CAM-B3LYP with the cc-pVXZ basis sets.

On the basis of these results (and the additional tests performed for the other molecules and reported in the Supporting Information), we do not employ diffuse functions in the CASPT2, NEVPT2, CC2, and TDDFT geometry optimization of the ground states and of the valence excited states of the molecules investigated here, and use the cc-pVTZ basis set as the default basis to compare the performance of the different methods.

**4.2. VMC Geometry Dependence on Basis Set and Jastrow Factor.** We investigate the dependence of the VMC geometries on the choice of basis set and Jastrow factor in the optimization of the ground and the $n \rightarrow \pi^*$ excited state of *s*-trans acrolein. As described in Section 2, we use correlated-consistent basis sets specifically constructed for the pseudopotentials we employ in the QMC calculations. Here, we test the double $\zeta$ basis (pVDZ), the triple basis for the heavy atoms combined with a double $\zeta$ for hydrogen (pVTZ′), and the triple basis set for all atoms (pVTZ). We also perform calculations augmenting these basis sets with diffuse functions on the heavy atoms. Furthermore, we employ two different Jastrow factors, that is, a two-body Jastrow factor ($\mathcal{J}_{2-\mathrm{body}}$) and a three-body Jastrow factor ($\mathcal{J}_{3-\mathrm{body}}$). We report the geometries optimized with a two-body Jastrow factor in Table 5 and those optimized with the addition of augmentation, also in combination with a three-body Jastrow factor, in the Supporting Information.

**Table 5. VMC Bond Lengths (Å) and Angles (deg) of *s*-Trans Acrolein[a]**

| VMC | pVDZ | pVTZ′ | pVTZ |
|---|---|---|---|
| | $1^1A'$ | | |
| C═O | 1.207(0) | 1.205(1) | 1.202(1) |
| C−C | 1.466(0) | 1.464(1) | 1.460(1) |
| C═C | 1.333(1) | 1.328(1) | 1.328(0) |
| $\theta$(C−C−C) | 118.93(8) | 120.89(6) | 120.25(5) |
| $\theta$(C−C−O) | 124.86(7) | 123.67(4) | 124.41(5) |
| | $1^1A''$ | | |
| C═O | 1.334(0) | 1.327(0) | 1.325(0) |
| C−C | 1.377(0) | 1.368(0) | 1.370(0) |
| C═C | 1.388(0) | 1.383(0) | 1.383(0) |
| $\theta$(C−C−C) | 123.76(1) | 122.57(1) | 121.89(0) |
| $\theta$(C−C−O) | 123.67(1) | 125.82(1) | 126.13(0) |

[a]We employ different basis sets, specifically constructed for our pseudopotentials, and a two-body Jastrow factor ($\mathcal{J}_{2-\mathrm{body}}$). The statistical error on the last digit is given in bracket.

In line with what observed for all other methods, we find that the bonds contract when the basis set is enlarged as also shown in Figure 4. Furthermore, also in VMC, the inclusion of diffuse

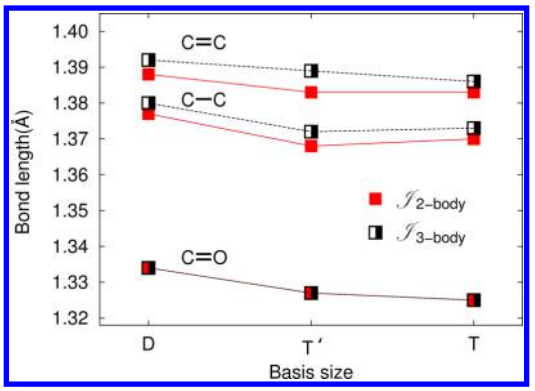


**Figure 4.** Convergence of the VMC bond lengths (Å) of *s*-trans acrolein in the $n \rightarrow \pi^*$ excited state computed with different basis sets and Jastrow factors. The statistical error bars are smaller than the symbol size.

functions slows down the convergence of the bond lengths with basis size (see Supporting Information). A difference with the other correlated approaches is that VMC displays a weaker dependence of the geometrical parameters on the basis set thanks to the presence of the Jastrow correlation function. We observe that the use of a valence triple and zeta; basis on the heavy atoms and a double on hydrogen (pVTZ′) leads to bond lengths, which are converged to better than 0.01 Å. Finally, introducing a three-body Jastrow factor gives a similar convergence, with respect to the basis as the two-body Jastrow factor, and leads to equivalent bond lengths within 0.003−0.006 Å. Therefore, as a good compromise between accuracy and computational cost, the VMC optimizations will be performed with the pVTZ′ basis set and a two-body Jastrow factor for all the other systems, since the use of a three-body Jastrow factor does not appreciably affect the results but significantly increases the time of the simulations.

**4.3. Acrolein.** The states of *s*-trans acrolein considered here are the ground state ($1^1A'$) and the $n \rightarrow \pi^*$ ($1^1A''$) and $\pi \rightarrow \pi^*$ excited states ($2^1A'$). The three states are optimized with planarity constraint ($C_s$ symmetry). The $2^1A'$ excited state is also studied in his twisted geometry, always maintaining $C_s$ symmetry. We also present a brief study of the ground and $n \rightarrow \pi^*$ excited-state geometries of the *s*-cis isomer of acrolein. In the following, when speaking about the double or single carbon−carbon bonds of acrolein, we always refer to the ground-state bond structure as depicted in Figure 5.

*4.3.1. Ground-State and n → π* Excited-State Geometries of s-Trans Acrolein.* The optimal geometries of *s*-trans acrolein in the ground and $n \rightarrow \pi^*$ excited states computed with CC2, CASPT2, NEVPT2, and VMC are given in Table 6. In the perturbation and the VMC optimization of the ground and

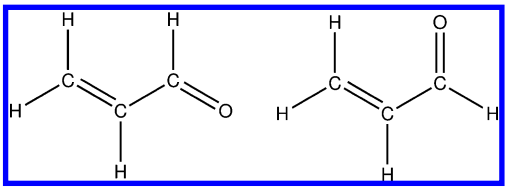


**Figure 5.** Structures of *s*-trans (left) and *s*-cis (right) acrolein.


dx.doi.org/10.1021/ct400876y | J. Chem. Theory Comput. XXXX, XXX, XXX−XXX

Table 6. CC2, CASPT2, NEVPT2, and VMC Bond Lengths (Å) and Angles (deg) of *s*-Trans Acrolein in the Ground State ($1^1A'$) and $n \rightarrow \pi^*$ Excited States ($1^1A''$)[a]

| | CC2 | CASPT2 | NEVPT2 | VMC |
|---|---|---|---|---|
| | | $1^1A'$ | | |
| C=O | 1.221 | 1.214 | 1.210 | 1.205(1) |
| C−C | 1.463 | 1.470 | 1.462 | 1.464(1) |
| C=C | 1.336 | 1.339 | 1.333 | 1.328(1) |
| $\theta$(C−C−C) | 120.00 | 120.36 | 120.33 | 120.89(6) |
| $\theta$(C−C−O) | 124.56 | 124.16 | 124.45 | 123.67(4) |
| | | $1^1A''$ | | |
| C=O | 1.368 | 1.336 | 1.328 | 1.327(0) |
| C−C | 1.370 | 1.377 | 1.371 | 1.368(0) |
| C=C | 1.383 | 1.392 | 1.385 | 1.383(0) |
| $\theta$(C−C−C) | 122.14 | 123.26 | 123.37 | 122.57(1) |
| $\theta$(C−C−O) | 127.15 | 124.54 | 124.79 | 125.82(1) |

[a]We employ a cc-pVTZ basis in the CC2 and PT2 calculations, and a pVTZ′ basis set in combination with a two-body Jastrow factor in VMC.

excited states, we use as reference wave function a CAS(6,5) expansion, where the active space comprises four $\pi$ orbitals on the conjugated carbon chain and a $\sigma$ orbital describing a lone pair in the direction orthogonal to the CO group. Our CASPT2 results for the ground and the $n \rightarrow \pi^*$ state are in good agreement with previous benchmark studies of *s*-trans acrolein based on a different CASPT2 approach (with the IPEA shift set to zero in the zero-order Hamiltonian).[49,82]

For the ground state, the optimal CC2, perturbation, and VMC geometries agree very well. The CASPT2 bond lengths are about 0.005 Å longer than the NEVPT2 values, and the CASPT2 and NEVPT2 results differ from the VMC ones by less than 0.01 and 0.005 Å, respectively. The CC2 method displays somewhat larger deviations from the other techniques in the CO bond, which is 0.015 Å longer than the VMC value. We note that, for the ground state, there exists a second CASSCF minimum very closed in energy and corresponding to a CAS(6,5) expansion, which includes a lone-pair orbital parallel to the CO group. The structural optimization performed at the CASPT2 level with this expansion leads to a geometry, which agrees to better than 0.001 Å[90] with the one of Table 6, indicating that the inclusion in the active space of either lone pair does not substantially influence the optimal ground-state geometry obtained in the subsequent correlated calculation.

As shown in the upper panel of Figure 6, we find a good agreement between the perturbation theories and VMC also in the excited state, with differences of the same order of magnitude as those observed for the ground state. In particular, the NEVPT2 bond lengths are again in excellent agreement with the VMC values, displaying deviations smaller than 0.003 Å. The agreement of CC2 with the other approaches is instead less satisfactory: While CC2 gives CC bond lengths, which are compatible with the VMC values, it overestimates the CO bond by as much as 0.04 Å. This behavior is in line with the general tendency of the method to overestimate the carbonyl bond in the $n \rightarrow \pi^*$ states of aldehydes.[26] A comparison with the SAC−CI calculations with the cc-pVTZ basis set of ref 50 reveals a poor performance also of the SAC−CI approach, which overestimates the CC bond, formerly single in the ground state, by 0.045 Å and underestimates the other CC bond by 0.025 Å, while the agreement on the CO bond length is rather good.

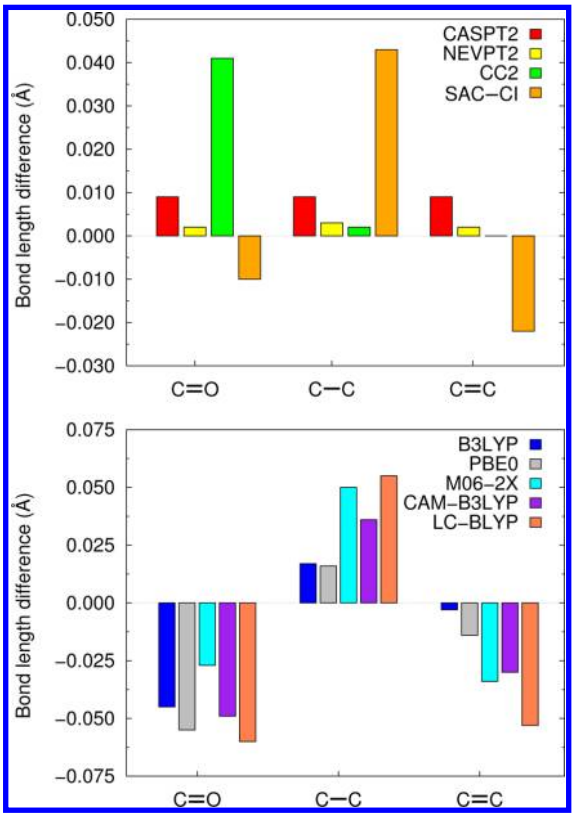


**Figure 6.** Bond-length differences (Å) between the geometries computed with different methods and the VMC reference for the $n \rightarrow \pi^*$ excited state of s-trans acrolein. The SAC−CI/cc-pVTZ values are from ref 50.

In the lower panel of Figure 6, we assess the quality of the TDDFT geometries against out VMC data. We employ a set of functionals which comprises some (B3LYP, PBE0, and CAM-B3LYP) considered also in previous benchmark studies.[19,25,82] The errors in the TDDFT bond lengths are compatible with those reported in ref 25, with the noteworthy exception of the CO bond. The apparent difference for this bond is, however, simply due to the use of a different reference geometry: The deviation of TDDFT with respect to VMC is about −0.05 Å for all the functionals considered here but increases to −0.1 Å when CC2 with the aug-cc-pVTZ basis set is taken as reference as in ref 25. Considering the near breakdown of the CC2 model in the description of the $n \rightarrow \pi^*$ excited state of acrolein (as well as of acetone and the propenoic acid anion) as also discussed in previous studies,[25,26] the choice of this method as reference for TDDFT geometry optimizations is surely not appropriate for this class of molecules. As for the performance of the TDDFT functionals, there is not a clear trend when increasing the amount of exact exchange in going from B3LYP (20%) to M06-2X (54%). While the use of the M06-2X halves the error on the CO bond, it significantly increases the deviations on the CC bonds by not sufficiently shortening/lengthening the bonds formerly single/double in the ground state. The use of the long-range corrected functionals CAM-B3LYP and LC-BLYP with either 65% and 100% exchange at long distances leads to significantly larger errors on the CC bonds and a comparable error on the CO bond as the hybrid BLYP and PBE0 functionals. We note here that, in all Figures throughout the paper, we employ VMC as our reference. This choice is mainly motivated by the fact that the NEVPT2 results are only available for acrolein, where they agree


dx.doi.org/10.1021/ct400876y | J. Chem. Theory Comput. XXXX, XXX, XXX−XXX

remarkably well with VMC, while the use of CASPT2 as reference poses a problem for the $\pi \rightarrow \pi^*$ state of acrolein as discussed below.

*4.3.2. Ground-State and n → π* Excited-State Geometries of s-Cis Acrolein.* In the literature, the cis configuration instead of the more stable trans configuration of acrolein (see Figure 5) has sometimes been adopted to benchmark the electronic excitations of various methods such as TDDFT[19] and CASPT2.[82] We expect that all considerations above about *s*-trans acrolein are directly transferable also to *s*-cis acrolein, and to demonstrate this, we optimize here the ground state and the $n \rightarrow \pi^*$ state of this isomer with the methods also used for *s*-trans acrolein.

We report the geometries obtained with the correlated methods in the Supporting Information. The ground-state geometries display an excellent agreement and, for the $n \rightarrow \pi^*$ excited state, we observe the same behavior noted for the trans isomer as shown in Figure 7 (upper panel): While the agreement

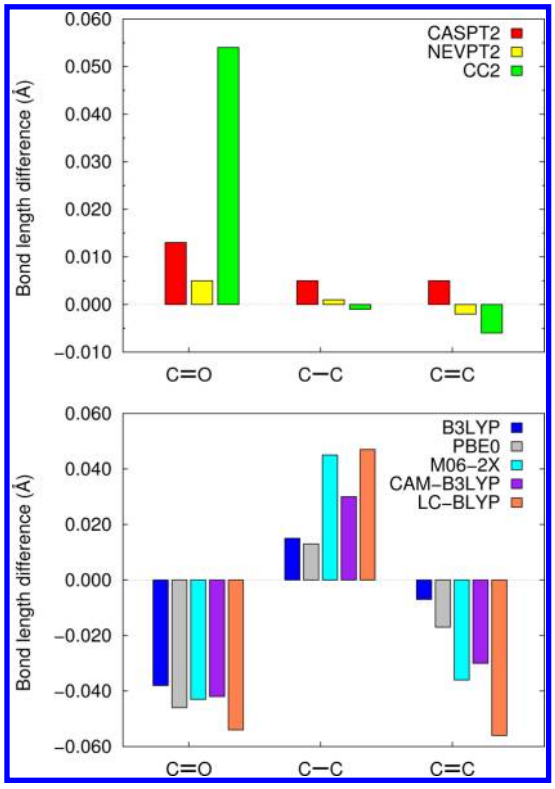


**Figure 7.** Bond-length differences (Å) between the geometries computed with different methods and the VMC reference for the $n \rightarrow \pi^*$ state of *s*-cis acrolein.

is very good between the perturbation theories and the VMC method, CC2 significantly overestimates the CO bond. The CC2 error on the CO bond is in fact somewhat larger than for the trans isomer.

For the functionals selected to test TDDFT, the errors with respect to the VMC optimized structure are of the same order of magnitude as for trans acrolein (see lower panel of Figure 7). Again, we observe a satisfactory performance of B3LYP and PBE0 for the CC bonds, while the CO bond length is underestimated by as much as 0.05 Å. The error on this bond is in the same range also for the other functionals considered here.

*4.3.3. Planar π → π* Excited-state Geometry of s-Trans Acrolein.* We optimize the geometry of *s*-trans acrolein also in the $\pi \rightarrow \pi^*$ state, a case which is less documented in the literature. The $\pi \rightarrow \pi^*$ transition leads to an excited state of the same symmetry as the ground state if planarity ($C_s$ symmetry) is imposed. For the planar optimization of this state, we limit the perturbation description to the CASPT2 method due to the limitations in code used to perform the NEVPT2 calculations as detailed in Section 2. In both the CASPT2 and VMC calculations, we employ a CAS(4,4) expansion over two bonding and two antibonding $\pi$ orbitals, which results in the bright excited state being the third root in the state-average CASSCF calculation.

The perturbation correction yields the energetic inversion of the two highest CASSCF roots, and the CASPT2 optimization following the second state leads to significantly different geometries if we use the single-state or the multistate flavor of CASPT2 (see Supporting Information). Even though the gap between the second and third state on the optimal geometry is about 0.012 hartree, we observe a strong mixing of the eigenvectors of the second and third roots in the multistate CASPT2 calculation, and therefore, a perturbation wave function dramatically different from the zero-order reference. The problem is not ameliorated if the active space is enlarged to include more $\pi^*$ orbitals. Therefore, we report below the CASPT2 geometry obtained with the smallest possible CAS(2,2) active space that leads to a straightforward multistate optimization of the second state but represents a computational expedient, which may be variationally rather poor.

In the VMC calculations, the use of a CAS(4,4) expansion over the $\pi$ orbitals in the determinantal component of the Jastrow-Slater wave function poses instead no problems. While the relevant transition is the third state at the CASSCF level as discussed above, the introduction of the Jastrow factor reorders the two highest roots. We perform the structural relaxation in the $\pi \rightarrow \pi^*$ state following the second state, whose wave function is obtained in a state-average optimization at the VMC level over three states. The state of interest remains the second one in the course of the geometrical optimization and, on the optimal geometry, is energetically separated from the higher state by about 0.013 hartree.

We report our CASPT2, CC2, and VMC geometries of the planar $\pi \rightarrow \pi^*$ excited state in Table 7 and compare them in

**Table 7. CC2, CASPT2, and VMC Geometries of the $\pi \rightarrow \pi^*$ ($2^1A'$) State of *s*-Trans Acrolein in the Planar Geometry[a]**

| | CC2 | CASPT2 | VMC |
|---|---|---|---|
| C=O | 1.286 | 1.279 | 1.266(2) |
| C−C | 1.433 | 1.444 | 1.443(1) |
| C=C | 1.436 | 1.429 | 1.428(1) |
| $\theta$(C−C−C) | 125.49 | 128.39 | 123.92(6) |
| $\theta$(C−C−O) | 121.30 | 119.27 | 121.64(1) |

[a]The CASPT2 geometry is obtained with a CAS(2,2) active space (see text).

Figure 8. We find that the optimal CASPT2 structure obtained with the reduced CAS(2,2) is in excellent agreement with the VMC geometry, the largest deviations being 0.013 Å for the CO bond and about 0.001 Åfor the CC bonds. The CC2 structure is also in satisfactory agreement with the VMC reference, only somewhat overestimating the CO bond by 0.02 Å, an error that is nevertheless smaller than the corresponding one for the $n \rightarrow \pi^*$ state. Finally, the agreement of the SAC−CI/cc-pVDZ data from ref 50 with the VMC geometry is particularly good for the CO


dx.doi.org/10.1021/ct400876y | J. Chem. Theory Comput. XXXX, XXX, XXX−XXX

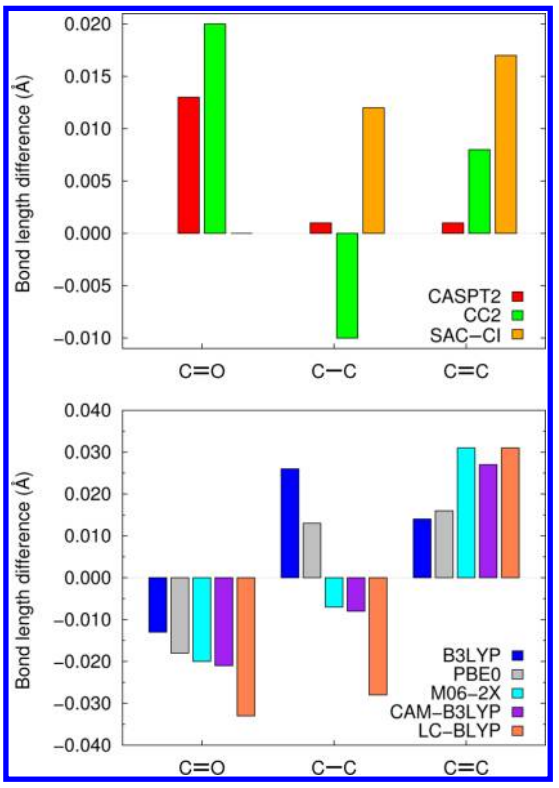


**Figure 8.** Bond-length differences (Å) between the geometries computed with different methods and the VMC reference for the $\pi \rightarrow \pi^*$ state of planar *s*-trans acrolein. The CASPT2 geometry is obtained with a CAS(2,2) active space (see text). The SAC−CI/cc-pVDZ values are from ref 50.

bond, while the CC bonds are slightly overestimated in SAC−CI. Finally, the TDDFT geometries are compared to VMC in Figure 8 (lower panel). Also, in the case of the $\pi \rightarrow \pi^*$ excitation, there is no clear correlation between the type of functional considered (e.g., dependence on the amount of exact exchange) and the quality of the corresponding optimized geometry. The overall performance of TDDFT is slightly better than for the $n \rightarrow \pi^*$ case and the general features that emerge from the comparison are the underestimation of the CO bond, with LC-BLYP giving the largest error of −0.033 Å, and the overestimation of the terminal CC bond.

*4.3.4. Twisted $\pi \rightarrow \pi^*$ Excited-state Geometry s-Trans Acrolein.* If the geometry in the $\pi \rightarrow \pi^*$ state of *s*-trans acrolein is optimized without imposing planarity, the minimum structure is twisted by about 90° around the terminal C═$CH_2$ bond, as shown in Figure 9. The $\pi \rightarrow \pi^*$ excited state of planar acrolein correlates adiabatically to a state with a strong diradical character in the twisted geometry. At the CASSCF level, the $\pi \rightarrow \pi^*$ wave function acquires a high weight on an up−down configuration with the HOMO orbital on the carbons in the plane and the LUMO on the terminal carbon of the twisted $CH_2$ group. To

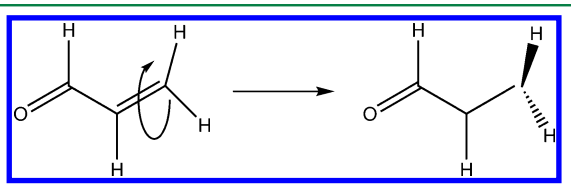


**Figure 9.** Schematic representation of the relaxation path of the $\pi \rightarrow \pi^*$ state of *s*-trans acrolein.

allow a comparison with previous SAC−CI calculations,[50] we keep the O−C−C frame planar and obtain a final structure with $C_s$ symmetry. The state with diradical character corresponds to the first root in the A″ irreducible representation, which is also the ground state of twisted acrolein, and active electrons in four orbitals, namely, three $\pi$ orbitals on the carbon chain in the molecular plane and the *p*-like $\sigma$ orbital resulting from the 90° rotation around the terminal C═$CH_2$ bond. We report our optimal perturbation and VMC geometries of twisted *s*-trans acrolein in the $1^1$A″ state in Table 8. The good agreement among

**Table 8. CASPT2, NEVPT2, and VMC Geometries of the $\pi \rightarrow \pi^*$ ($1^1$A″) State of *s*-Trans Acrolein in the Twisted Geometry**

| | CASPT2 | NEVPT2 | VMC |
|---|---|---|---|
| C═O | 1.232 | 1.226 | 1.218(0) |
| C−C | 1.436 | 1.431 | 1.427(1) |
| C═C | 1.454 | 1.449 | 1.444(0) |
| $\theta$(C−C−C) | 123.66 | 123.97 | 123.45(5) |
| $\theta$(C−C−O) | 122.82 | 122.96 | 122.80(4) |
| Θ (C−C−C−H) | 92.14 | 92.2 | 93.14(8) |

the CASPT2, NEVPT2, and VMC structures is confirmed also for this state of acrolein. As shown in Figure 10, both

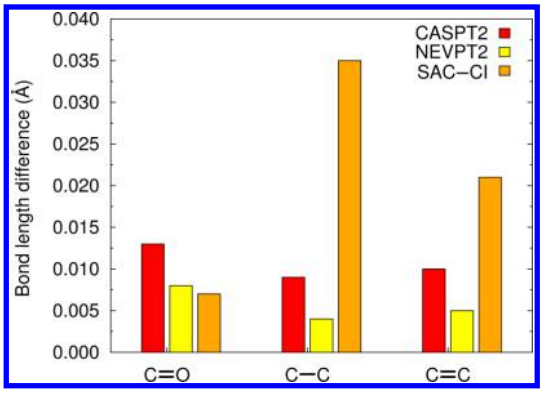


**Figure 10.** Bond-length differences (Å) between the geometries computed with different methods and the VMC reference for the $\pi \rightarrow \pi^*$ state of *s*-trans acrolein in the twisted geometry.

perturbation methods only slightly overestimate the VMC bond lengths with the largest discrepancy of 0.013 Å being for the CO bond and CASPT2. On the other hand, the SAC−CI/cc-pVDZ structure from ref 50 only agrees with VMC on the CO bond while the CC bonds are overestimated with a large error of about 0.035 Å for the C—C bond and 0.02 Å for the C═C bond.

**4.4. Acetone.** To optimize the ground-state geometry of acetone, we impose $C_{2v}$ symmetry and, in the $n \rightarrow \pi^*$ state, consider two conformations, one with the same symmetry as the ground state and the other one having $C_s$ symmetry as a consequence of the pyramidalization of the central carbon atom out of the molecular plane. In the excited state of the $C_{2v}$ and $C_s$ conformations, the geometry is therefore optimized for the first root in the $A_2$ and the A″ irreducible representation, respectively. This second nonplanar structure corresponds to a true minimum for the $n \rightarrow \pi^*$ state.

The ground- and excited-state geometries obtained with the correlated methods are listed in Table 9 and compared in Figure 11. As perturbation approaches, we only employ the CASPT2 method to optimize the excited-state structure due to the difficulties in the use of NEVPT2 as explained in Section 2. In the


dx.doi.org/10.1021/ct400876y | J. Chem. Theory Comput. XXXX, XXX, XXX−XXX

**Table 9. CC2, CASPT2, NEVPT2, and VMC Bond Lengths (Å) and Angles (deg) of Acetone in the Ground State ($1^1A_1$) and in the $n \rightarrow \pi^*$ Excited ($1^1A_2$ and $1^1A''$) States Optimized Either in $C_{2v}$ or $C_S$ Symmetry[a]**

| | CC2 | CASPT2 | NEVPT2 | VMC |
|---|---|---|---|---|
| | | $1^1A_1$ ($C_{2v}$) | | |
| C═O | 1.222 | 1.214 | 1.211 | 1.205(0) |
| C−C | 1.504 | 1.509 | 1.501 | 1.502(1) |
| $\theta$(C−C−O) | 121.93 | 121.91 | 121.89 | 119.80(2) |
| | | $1^1A_2$ ($C_{2v}$) | | |
| C═O | 1.422 | 1.360 | | 1.348(1) |
| C−C | 1.473 | 1.487 | | 1.481(1) |
| $\theta$(C−C−O) | 116.24 | 116.86 | | 118.99(4) |
| | | $1^1A''$ ($C_S$) | | |
| C═O | 1.404 | 1.350 | | 1.344(1) |
| C−C | 1.477 | 1.496 | | 1.489(1) |
| $\theta$(C−C−O) | 112.63 | 112.75 | | 112.52(8) |
| $\Theta$(H−C−C−O) | 55.37 | 52.25 | | 52.16(13) |

[a]We employ a cc-pVTZ basis in the CC2 and PT2 calculations, and a pVTZ′ basis set in combination with a two-body Jastrow factor in VMC.

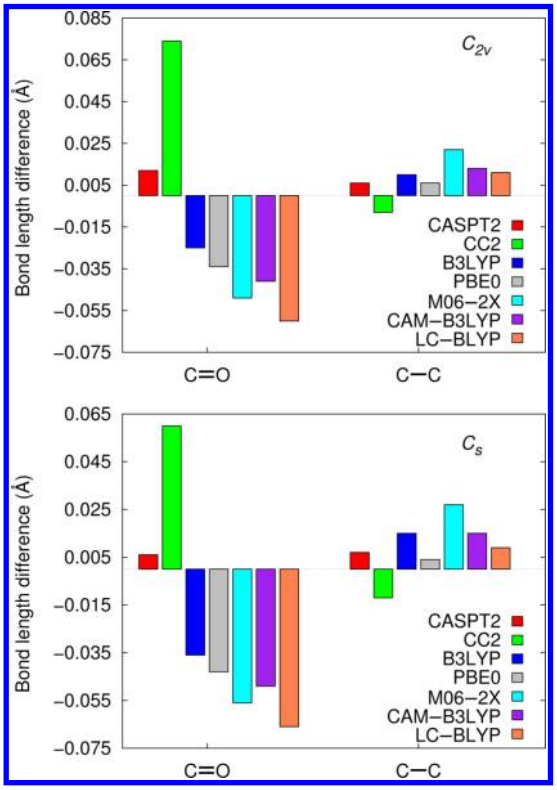


**Figure 11.** Differences in the bond lengths (Å) computed with different methods with respect to the VMC values for the $n \rightarrow \pi^*$ state of acetone in the $C_{2v}$ (top) and $C_s$(bottom) conformations.

CASPT2 and VMC calculations, we use a CAS(4,3) expansion as reference wave function, where the active space includes the lone pair on the oxygen and the bonding and antibonding $\pi$ orbitals on the CO bond.[91] In the ground state, the CC2, CASPT2, and VMC methods yield very close geometries, with the largest deviation of 0.017 Å being between CC2 and VMC on the CO bond. For the excited states, the CASPT2 and VMC optimal structures are in very good agreement, always differing by less than 0.01 Å. Also, for the $n \rightarrow \pi^*$ state of this molecule, the biggest difference is observed for the CO bond length computed with the CC2 method, which deviates from the VMC value by as much as 0.074 Å when planar symmetry is imposed (see upper panel in Figure 11).

Similarly to the acrolein case, all TDDFT functionals tend to underestimate the CO bond length of acetone with respect to the optimized VMC structure, giving errors as large as 0.06 Å for the LC-BLYP functional, as also shown in Figure 11. Given the good agreement between CASPT2 and VMC, the TDDFT deviations obtained here are comparable to the ones reported in an older benchmark publication[19] using CASPT2 as reference. On the other hand, the choice of CC2 as reference as in the more recent study of ref. 25 is not recommended since the large error of CC2 for the CO bond with respect to either CASPT2 or VMC will incorrectly affect the comparison.

**4.5. Methylenecyclopropene.** We optimize the geometry of methylenecyclopropene in the ground and the $\pi \rightarrow \pi^*$ excited state maintaining planarity ($C_{2v}$ symmetry), so the two states have $1^1A_1$ and $1^1B_2$ symmetry, respectively. We note that the planar geometry does not correspond to a minimum for this excited state since a twisting of 90° around the exocyclic C═$CH_2$ bond is expected to stabilize the state in analogy to what happens for acrolein.[92] Since we are also interested in a comparison with the CC2 and TDDFT approaches, which cannot describe diradical systems as noted above, we limit here our study to the planar $\pi \rightarrow \pi^*$ state of methylenecyclopropene. The atomic labels for this molecule are specified in Figure 12.

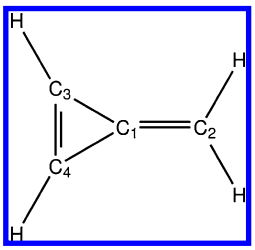


**Figure 12.** Methylenecyclopropene with atomic labels.

We present the perturbation, CC2, and VMC ground- and excited-state geometries in Table 10. In the perturbation and VMC calculations, we construct the reference wave functions of

**Table 10. CC2, CASPT2, NEVPT2, and VMC Bond Lengths (Å) and Angles (deg) of the Ground ($1^1A_1$) and the $\pi \rightarrow \pi^*$ Excited ($1^1B_2$) State of Planar Methylenecyclopropene[a]**

| | CC2 | CASPT2 | NEVPT2 | VMC |
|---|---|---|---|---|
| | | $1^1A_1$ | | |
| $C_1$═$C_2$ | 1.328 | 1.331 | 1.327 | 1.324(0) |
| $C_1$−$C_3$ | 1.438 | 1.442 | 1.434 | 1.434(0) |
| $C_4$═$C_3$ | 1.325 | 1.324 | 1.319 | 1.316(1) |
| $\theta$($C_2$−$C_1$−$C_3$) | 152.56 | 152.66 | 152.62 | 152.98(4) |
| $\theta$($C_1$−$C_3$−$C_4$) | 62.56 | 62.67 | 62.62 | 62.63(3) |
| | | $1^1B_2$ | | |
| $C_1$═$C_2$ | 1.457 | 1.461 | | 1.456(1) |
| $C_1$−$C_3$ | 1.349 | 1.360 | | 1.351(1) |
| $C_4$═$C_3$ | 1.512 | 1.496 | | 1.483(0) |
| $\theta$($C_2$−$C_1$−$C_3$) | 145.90 | 146.64 | | 146.66(2) |
| $\theta$($C_1$−$C_3$−$C_4$) | 55.90 | 56.64 | | 56.66(3) |

[a]We employ a cc-pVTZ basis set in the CC2 and PT2 calculations, and a pVTZ′ basis set in combination with a two-body Jastrow factor in VMC.


dx.doi.org/10.1021/ct400876y | J. Chem. Theory Comput. XXXX, XXX, XXX−XXX

both states as a CAS(4,4) expansion over two bonding and two antibonding $\pi$ orbitals. We find that the ground-state perturbation and CC2 geometries are in very good agreement with the VMC structures, with all deviations being smaller than 0.01 Å. These ground-state structures are also compatible with the corresponding SAC−CI/cc-pVDZ geometry of ref 50. In the excited state, we observe an inversion of the single and double bonds, which is well reproduced by all techniques. Also for this state, the VMC and CASPT2 structures agree very well as shown in Figure 13 (upper panel). The comparison with CC2 and

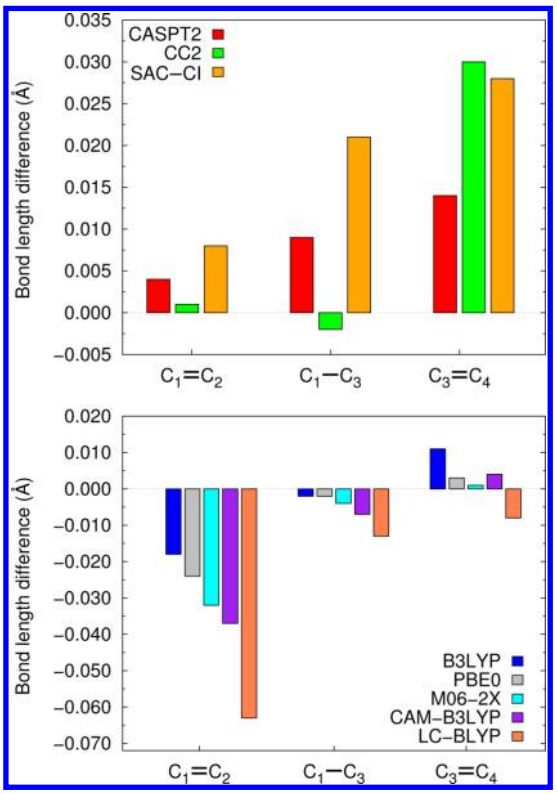


**Figure 13.** Bond-length differences (Å) between the geometries computed with different methods and the VMC reference for the $\pi \rightarrow \pi^*$ ($1^1B_2$) state of planar methylenecyclopropene.

SAC−CI reveals instead bigger errors in correspondence of the $C_3{=}C_4$ bond in the ring, which both techniques overestimate by about 0.025 Å. The excited-state description of this part of the molecule is expected to be more critical since the excitation strongly localizes the electrons on the ring atoms.[93] On the other hand, TDDFT displays the opposite behavior, giving smaller deviations from VMC on this bond and non-negligible errors on $C_1{=}C_2$. Also for this molecule, the best performance is obtained with the hybrid B3LYP and PBE0 functionals (see lower panel in Figure 13).

**4.6. Propenoic Acid Anion.** The last molecule considered in this study is the propenoic acid anion, for which we compute the structures of the ground state and the first singlet excited state corresponding to the $n \rightarrow \pi^*$ excitation. The molecular structure and the relevant atomic labels are given in Figure 14.

We report the CC2, CASPT2, and VMC geometrical parameters of the propenoic acid anion in Table 11. In the ground-state optimization with the perturbation and VMC approaches, we choose a CASSCF wave function, which correlates eight electrons in six orbitals, five orbitals of $\pi$ character, and one $\sigma$ orbital describing the lone pair on one

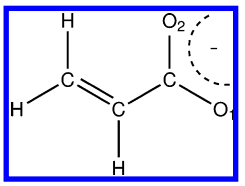


**Figure 14.** Propenoic acid anion with atomic labels.

**Table 11. C2, CASPT2, NEVPT2, and VMC Bond Lengths (Å) and Angles (deg) of the Ground and $n \rightarrow \pi^*$ Excited States of the Propenoic Acid Anion**[a]

| | CC2 | CASPT2 | VMC |
|---|---|---|---|
| | $1^1A'$ | | |
| $C{-}O_1$ | 1.265 | 1.260 | 1.245(1) |
| $C{-}O_2$ | 1.261 | 1.253 | 1.241(0) |
| C−C | 1.521 | 1.531 | 1.526(1) |
| C=C | 1.335 | 1.338 | 1.324(0) |
| $\theta(O_1{-}C{-}C)$ | 114.02 | 114.00 | 113.95(5) |
| $\theta(C{-}C{-}C)$ | 123.48 | 123.68 | 124.03(6) |
| $\theta(O_1{-}C{-}O_2)$ | 129.59 | 129.69 | 129.72(4) |
| | $1^1A''$ | | |
| $C{-}O_1$ | 1.311 | 1.309 | 1.291(1) |
| $C{-}O_2$ | 1.331 | 1.299 | 1.284(1) |
| C−C | 1.385 | 1.387 | 1.379(0) |
| C=C | 1.415 | 1.412 | 1.401(0) |
| $\theta(O_1{-}C{-}C)$ | 130.41 | 128.39 | 128.33(7) |
| $\theta(C{-}C{-}C)$ | 123.43 | 124.70 | 124.49(7) |
| $\theta(O_1{-}C{-}O_2)$ | 102.32 | 103.98 | 107.18(7) |

[a]We employ a cc-pVTZ basis set in the CC2 and CASPT2 calculations, and a pVTZ′ basis set in combination with a two-body Jastrow factor in VMC.

oxygen. At the CASPT2 level, the ground-state energy with a CAS(8,6) expansion is optimal if the $\sigma$ orbital is on the $C{-}O_1$ bond, and it is unfortunately not possible to stabilize a larger CAS also including the lone pair on the $C{-}O_2$ bond. The optimal ground-state geometries are characterized by almost equal CO bond lengths and are rather similar at all levels of theory. At the CC2 level, the CO bonds are slightly longer than the CASPT2 ones and therefore further away from the VMC values.

In the $n \rightarrow \pi^*$ state, one can construct two CAS(8,6) expansions by including the $\sigma$ orbital either on the $C{-}O_1$ or on the $C{-}O_2$ bond, as well as a CAS(10,7) active space comprising both lone pairs. These reference wave functions lead to very different CASPT2 and VMC geometries. If we employ the CAS(8,6) expansions, which give rather close CASPT2 energies on the ground-state geometry, we obtain a differential elongation of the $C{-}O_1$ and $C{-}O_2$ bonds, where the bond elongating is the one associated to the lone pair included in the active space. The geometry with a longer $C{-}O_2$ is consistent with the one reported in a previous CASPT2 study with the same active space.[49] Chemically, it is, however, unclear why the excited-state geometry should display a differential elongation of the two CO bonds, which is moreover crucially dependent on the choice of the $\sigma$ orbital included in the active space. Therefore, we perform also a CASPT2 optimization with both lone pairs in a CAS(10,7) expansion.

As shown in Table 11, the use of the CAS(10,7) reference yields the expected behavior within CASPT2 and VMC: Both CO bonds are equally elongated with respect to the ground-state geometry by about 0.04−0.05 Å. We note that the use of a CAS(10,7) active space always leads to the same CASPT2


dx.doi.org/10.1021/ct400876y | J. Chem. Theory Comput. XXXX, XXX, XXX−XXX

minimum with equal CO bond lengths independently of the starting geometry being the ground-state or the two CAS(8,6) excited-state structures. Within VMC, the optimization with a CAS(10,7) leads instead to distinct minima if we start from these different geometries. Two minima are characterized by a differential elongation of the CO bonds while the other one has equal CO bond lengths and is lower in energy by about 7 mHartree. This optimal excited-state VMC structure is similar to the CASPT2 one, but as in the ground state, we observe differences of about 0.02 Å on the CO bonds. In the excited state, CC2 yields a similar lengthening of both CO bonds as observed at the CASPT2 and VMC level (See Figure 15). The biggest

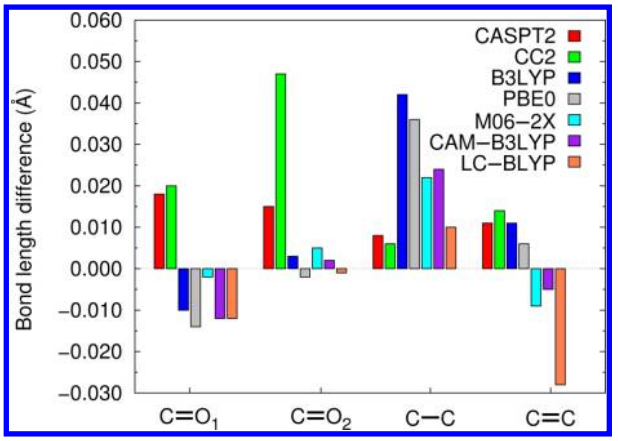


**Figure 15.** Bond-length differences (Å) between the geometries computed with different methods and the VMC reference for the $n \rightarrow \pi^*$ state of propenoic acid anion.

difference with the other correlated approaches is the excessive lengthening of the C−$O_2$ bond, which is 0.03 and 0.05 Å longer than the CASPT2 and VMC values, respectively. Finally, the geometries optimized at the TDDFT level share the common feature of having CO bonds of equal length which are very close to the VMC values, while bigger differences are observed for the C−C bond.

## 5. CONCLUSIONS

In this paper, we have presented a thorough investigation of the performance of a variety of first-principle approaches in optimizing the geometries of a set of small organic chromophores, with particular focus on their excited-state structures. The primary goal was to assess the accuracy of the VMC geometries through a detailed comparison with those obtained with other highly correlated approaches such as multireference perturbation approaches (CASPT2 and NEVPT2), coupled cluster (CC2) and SAC−CI, which have been used in previous benchmark studies of TDDFT or other correlated approaches.

For this aim, we revisited the perturbation calculations for these molecules with special emphasis on the construction of the reference wave function since the choice of active space may significantly affect the excited-state optimal geometry as in the case of the propenoic acid anion.

As shown in Figure 16, the level of agreement between the different methods and VMC can be discussed in terms of the maximum absolute deviations (MXAD) with respect to the VMC excited-state bond lengths. For the perturbation theories and CC2, the MXAD occurs for the CO bond of the carbonyl compounds and for the double CC bond in the ring of MCP,

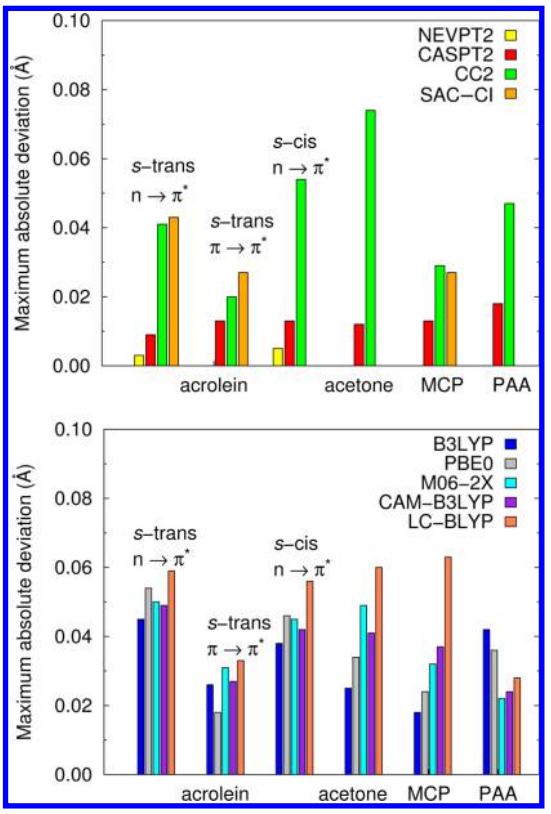


**Figure 16.** Maximum absolute deviations (Å) on the bond lengths in the excited state with respect to the VMC optimal geometries.

while we find that SAC−CI consistently gives a worse description of the CC bond lengths. We observe that the VMC and perturbation structures are always very close: The MXADs are extremely small at the NEVPT2 level and consistently around 0.013 Å within CASPT2, with the only exception of the more problematic case of the propenoic acid anion with its bigger error of about 0.018 Å. With maximum absolute deviations of 0.04−0.075 Å, the comparison with CC2 confirms the lack of accuracy of this method in the description of the CO bond in the $n \rightarrow \pi^*$ excited states as already reported in ref 26. CC2 is instead able to provide a somewhat better description of the $\pi \rightarrow \pi^*$ excited states of acrolein and MCP, where the MXADs are about 0.02−0.03 Å. The maximum errors on the SAC−CI geometries are of the same order of magnitude as those on the CC2 structures.

At the TDDFT level, most functionals give the largest errors on the CO bond of the carbonyl compounds in the $n \rightarrow \pi^*$ excited states, with the exception of the propenoic acid anion where all functionals fail on the CC bonds. As regards the $\pi \rightarrow \pi^*$ excitations, the MXAD for the different functionals is always on the exocyclic double bond of MCP while it occurs on different bonds of acrolein. Manifestly, it is not possible to identify a clear correlation between the defining features of the different functional investigated (e.g., amount of exact exchange) and the accuracy of the geometry obtained. Furthermore, while the poorest results are obtained with the LC-BLYP functional, it is not straightforward to pinpoint a single functional as the one offering the best overall performance in the optimization of the excited-state structures of these molecules.

In conclusion, our study demonstrates that QMC (also in its simplest VMC variant) can be successfully employed as a robust method for the accurate optimization of ground- and excited-state structures also in cases where other correlated or TDDFT


dx.doi.org/10.1021/ct400876y | J. Chem. Theory Comput. XXXX, XXX, XXX−XXX

methods fail. Thanks to its favorable computational scaling with the system size, QMC represents therefore a promising alternative to other methods ordinarily employed in quantum chemistry for the structural study also of more complex molecules.

## ■ ASSOCIATED CONTENT

### Supporting Information

Coordinates optimized with CASPT2 for all molecules and states. Convergence studies with basis sets and, for the quantum Monte Carlo calculations, with the form of the Jastrow factor. This material is available free of charge via the Internet at http://pubs.acs.org.

## ■ AUTHOR INFORMATION

### Corresponding Author

*E-mail: c.filippi@utwente.nl.

### Notes

The authors declare no competing financial interest.

## ■ ACKNOWLEDGMENTS

R.G. is supported by an ECHO grant (712.012.005) of The Netherlands Organization for Scientific Research (NWO). We thank S. Moroni and C. Amovilli for useful discussions. Support by COST Action CODECS is acknowledged.

## ■ REFERENCES

(1) Casida, M. *J. Mol. Struct. (THEOCHEM)* **2009**, *914*, 3−18.
(2) Casida, M. E.; Huix-Rotllant, M. *Annu. Rev. Phys. Chem.* **2012**, *63*, 287−323.
(3) Marques, M.; Maitra, T. N.; Nogueira, F. M. S.; Gross, E.; Rubio, A. *Fundamentals of Time-Dependent Density Functional Theory*; Springer: Heidelberg, 2012; pp 53−99.
(4) Dreuw, A.; Weisman, J. L.; Head-Gordon, M. *J. Chem. Phys.* **2003**, *119*, 2943−2947.
(5) Casida, M. E. *J. Chem. Phys.* **2005**, *122*, 054111−054120.
(6) Yanai, T.; Tew, D. P.; Handy, N. C. *Chem. Phys. Lett.* **2004**, *393*, 51−57.
(7) Iikura, H.; Tsuneda, T.; Yanai, T.; Hirao, K. *J. Chem. Phys.* **2001**, *115*, 3540−3544.
(8) Tawada, Y.; Tsuneda, T.; Yanagisawa, S.; Yanai, T.; Hirao, K. *J. Chem. Phys.* **2004**, *120*, 8425−8433.
(9) Chiba, M.; Tsuneda, T.; Hirao, K. *J. Chem. Phys.* **2006**, *124*, 144106−144117.
(10) Vydrov, O. A.; Heyd, J.; Krukau, A. V.; Scuseria, G. E. *J. Chem. Phys.* **2006**, *125*, 074106−074115.
(11) Vydrov, O. A.; Scuseria, G. E. *J. Chem. Phys.* **2006**, *125*, 234109−234118.
(12) Chai, J.-D.; Head-Gordon, M. *J. Chem. Phys.* **2008**, *128*, 084106−084121.
(13) Chai, J.-D.; Head-Gordon, M. *Phys. Chem. Chem. Phys.* **2008**, *10*, 6615−6620.
(14) Furche, F.; Ahlrichs, R. *J. Chem. Phys.* **2002**, *117*, 7433−7448.
(15) Scalmani, G.; Frisch, J. M.; Mennucci, B.; Tomasi, J.; Cammi, R.; Barone, V. *J. Chem. Phys.* **2006**, *124*, 094107−094122.
(16) Rohrdanz, M. A.; Herbert, M. J. *J. Chem. Phys.* **2008**, *129*, 034107−034115.
(17) Jacquemin, D.; Perpète, E. A.; Scuseria, G. E.; Ciofini, I.; Adamo, C. *Chem. Phys. Lett.* **2008**, *465*, 226−229.
(18) Jacquemin, D.; Wathelet, V.; Perpète, E. A.; Adamo, C. *J. Chem. Theory Comput.* **2009**, *5*, 2420−2435.
(19) Guido, C. A.; Jacquemin, D.; Adamo, C.; Mennucci, B. *J. Phys. Chem. A* **2010**, *114*, 13402−13410.
(20) Send, R.; Kühn, M.; Furche, F. *J. Chem. Theory Comput.* **2011**, *7*, 2376−2386.
(21) Leang, S. S.; Zahariev, F.; Gordon, M. S. *J. Chem. Phys.* **2012**, *136*, 104101−104113.
(22) Jacquemin, D.; Planchat, A.; Adamo, C.; Mennucci, B. *J. Chem. Theory Comput.* **2012**, *8*, 2359−2372.
(23) Bousquet, D.; Fukuda, R.; Maitarad, P.; Jacquemin, D.; Ciofini, A.; Adamo, C.; Ehara, M. *J. Chem. Theory Comput.* **2013**, *9*, 2368−2379.
(24) Laurent, A. D.; Jacquemin, D. *Int. J. Quantum Chem.* **2013**, *113*, 2019−2039.
(25) Guido, C. A.; Knecht, S.; Kongsted, J.; Mennucci, B. *J. Chem. Theory Comput.* **2013**, *9*, 2209−2220.
(26) Köhn, A.; Hätting, C. *J. Chem. Phys.* **2003**, *119*, 5021−5037.
(27) Foulkes, W. M. C.; Mitas, L.; Needs, R. J.; Rajagopal, G. *Rev. Mod. Phys.* **2001**, *73*, 33−83.
(28) Kolorenc, J.; Mitas, L. *Rep. Prog. Phys.* **2011**, *74*, 026502−026530.
(29) Austin, B. M.; Zubarev, D. Y.; Lester, W. A. *Chem. Rev.* **2012**, *112*, 263−288.
(30) Schautz, F.; Filippi, C. *J. Chem. Phys.* **2004**, *120*, 10931−10941.
(31) Schautz, F.; Buda, F.; Filippi, C. *J. Chem. Phys.* **2004**, *121*, 5836−5844.
(32) Drummond, N.; Williamson, A.; Needs, R.; Galli, G. *Phys. Rev. Lett.* **2005**, *95*, 096801−096805.
(33) Cordova, F.; Doriol, L. J.; Ipatov, A.; Casida, M. E.; Filippi, C.; Vela, A. *J. Chem. Phys.* **2007**, *127*, 164111.
(34) Tapavicza, E.; Tavernelli, I.; Rothlisberger, U.; Filippi, C.; Casida, M. E. *J. Chem. Phys.* **2008**, *129*, 124108.
(35) Zimmerman, P. M.; Toulouse, J.; Zhang, Z.; Musgrave, C. B.; Umrigar, C. J. *J. Chem. Phys.* **2009**, *131*, 124103−124110.
(36) Filippi, C.; Zaccheddu, M.; Buda, F. *J. Chem. Theory Comput.* **2009**, *5*, 2074−2087.
(37) Valsson, O.; Filippi, C. *J. Chem. Theory Comput.* **2010**, *6*, 1275−1292.
(38) Send, R.; Valsson, O.; Filippi, C. *J. Chem. Theory Comput.* **2011**, *7*, 444−455.
(39) Filippi, C.; Buda, F.; Guidoni, L.; Sinicropi, A. *J. Chem. Theory Comput.* **2012**, *8*, 112−124.
(40) Valsson, O.; Angeli, C.; Filippi, C. *Phys. Chem. Chem. Phys.* **2012**, *14*, 11015−11020.
(41) Valsson, O.; Campomanes, P.; Tavernelli, I.; Rothlisberger, U.; Filippi, C. *J. Chem. Theory Comput.* **2013**, *9*, 2441−2454.
(42) Ghigo, G.; Roos, B. O.; Malmqvist, P.-Å. *Chem. Phys. Lett.* **2004**, *396*, 142−149.
(43) Angeli, C.; Cimiraglia, R.; Evengelisti, S.; Leininger, T.; Malrieu, J.-P. *J. Chem. Phys.* **2001**, *114*, 10252−10264.
(44) Attaccalite, C.; Sorella, S. *Phys. Rev. Lett.* **2008**, *100*, 114501−114505.
(45) Sorella, S.; Capriotti, L. *J. Chem. Phys.* **2010**, *133*, 234111−234121.
(46) Barborini, M.; Guidoni, L. *J. Chem. Phys.* **2012**, *137*, 224309−224318.
(47) Saccani, S.; Filippi, C.; Moroni, S. *J. Chem. Phys.* **2013**, *138*, 084109−084114.
(48) Umrigar, C. J.; Toulouse, J.; Filippi, C.; Sorella, S.; Hennig, R. G. *Phys. Rev. Lett.* **2007**, *98*, 110201−110203.
(49) Page, S. C.; Olivucci, M. *J. Comput. Chem.* **2003**, *24*, 298−309.
(50) Cammi, R.; Fukuda, R.; Ehara, M.; Nakatsuij, H. *J. Chem. Phys.* **2010**, *133*, 024104−024128.
(51) Frisch, M. J.; Trucks, G. W.; Schlegel, H. B.; Scuseria, G. E.; Robb, M. A.; Cheeseman, J. R.; Scalmani, G.; Barone, V.; Mennucci, B.; Petersson, G. A.; Nakatsuji, H.; Caricato, M.; Li, X.; Hratchian, H. P.; Izmaylov, A. F.; Bloino, J.; Zheng, G.; Sonnenberg, J. L.; Hada, M.; Ehara, M.; Toyota, K.; Fukuda, R.; Hasegawa, J.; Ishida, M.; Nakajima, T.; Honda, Y.; Kitao, O.; Nakai, H.; Vreven, T.; Montgomery, J. A., Jr.; Peralta, J. E.; Ogliaro, F.; Bearpark, M.; Heyd, J. J.; Brothers, E.; Kudin, K. N.; Staroverov, V. N.; Kobayashi, R.; Normand, J.; Raghavachari, K.; Rendell, A.; Burant, J. C.; Iyengar, S. S.; Tomasi, J.; Cossi, M.; Rega, N.; Millam, J. M.; Klene, M.; Knox, J. E.; Cross, J. B.; Bakken, V.; Adamo, C.; Jaramillo, J.; Gomperts, R.; Stratmann, R. E.; Yazyev, O.; Austin, A. J.; Cammi, R.; Pomelli, C.; Ochterski, J. W.; Martin, R. L.; Morokuma, K.; Zakrzewski, V. G.; Voth, G. A.; Salvador, P.; Dannenberg, J. J.; Dapprich,

S.; Daniels, A. D.; Farkas, Ö.; Foresman, J. B.; Ortiz, J. V.; Cioslowski, J.; Fox, D. J. *Gaussian 09* Revision A.02; Gaussian Inc.: Wallingford, CT, 2009.
(52) Becke, A. D. *Phys. Rev. A* **1988**, *38*, 3098−3100.
(53) Lee, C.; Yang, W.; Parr, R. G. *Phys. Rev. B* **1988**, *37*, 785−789.
(54) Becke, A. D. *J. Chem. Phys.* **1993**, *98*, 5648−5652.
(55) Stephens, P. J.; Devlin, F. J.; Chabalowski, C. F.; Frisch, M. J. *J. Phys. Chem.* **1994**, *98*, 11623−11627.
(56) Perdew, J. P.; Burke, K.; Ernzerhof, M. *J. Chem. Phys.* **1996**, *105*, 9982−9985.
(57) Adamo, C.; Barone, V. *J. Chem. Phys.* **1999**, *110*, 6158−6170.
(58) Ernzerhof, M.; Scuseria, G. E. *J. Chem. Phys.* **1999**, *110*, 5029−5036.
(59) Zhao, Y.; Truhlar, D. *Theor. Chem. Acc.* **2008**, *120*, 215−241.
(60) Christiansen, O.; Koch, H.; Jørgensen, P. *Chem. Phys. Lett.* **1995**, *243*, 409.
(61) Hättig, C.; Weigend, F. *J. Chem. Phys.* **2000**, *113*, 5154−5161.
(62) Hättig, C.; Köhn, A. *J. Chem. Phys.* **2002**, *117*, 6939−6951.
(63) Hättig, C. *Adv. Quantum Chem.* **2005**, *50*, 37−60.
(64) CFOUR, Coupled-Cluster techniques for Computational Chemistry, a quantum-chemical program package by J.F. Stanton, J. Gauss, M.E. Harding, P.G. Szalay with contributions from A.A. Auer, R.J. Bartlett, U. Benedikt, C. Berger, D.E. Bernholdt, Y.J. Bomble, L. Cheng, O. Christiansen, M. Heckert, O. Heun, C. Huber, T.-C. Jagau, D. Jonsson, J. Jusélius, K. Klein, W.J. Lauderdale, D.A. Matthews, T. Metzroth, L.A. Mück, D.P. O'Neill, D.R. Price, E. Prochnow, C. Puzzarini, K. Ruud, F. Schiffmann, W. Schwalbach, S. Stopkowicz, A. Tajti, J. Vázquez, F. Wang, J.D. Watts and the integral packages MOLECULE (J. Almlöf and P.R. Taylor), PROPS (P.R. Taylor), ABACUS (T. Helgaker, H.J. Aa. Jensen, P. Jørgensen, and J. Olsen), and ECP routines by A. V. Mitin and C. van Wüllen. For the current version, see http://www.cfour.de (accessed July 12, 2012).
(65) Karlström, G.; Lindh, R.; Malmqvist, P.-Å.; Roos, B. O.; Ryde, U.; Veryazov, V.; Widmark, P.-O.; Cossi, M.; Schimmelpfennig, B.; Neogrady, P.; Seijo, L. *Comput. Mater. Sci.* **2003**, *28*, 222−239.
(66) Andersson, K.; Malmqvist, P.-A.; Roos, B. O.; Sadlej, A. J.; Wolinski, K. *J. Phys. Chem.* **1990**, *94*, 5483−5488.
(67) Andersson, K.; Malmqvist, P.-A.; Roos, B. O. *J. Chem. Phys.* **1992**, *96*, 1218−1226.
(68) Angeli, C.; Cimiraglia, R.; Malrieu, J.-P. *Chem. Phys. Lett.* **2001**, *350*, 297−305.
(69) Angeli, C.; Cimiraglia, R.; Malrieu, J.-P. *J. Chem. Phys.* **2002**, *117*, 9138−9153.
(70) Neese, F. *Comput. Mol. Sci.* **2012**, *2*, 73−78.
(71) CHAMP is a quantum Monte Carlo program package written by Umrigar, C. J.; Filippi, C. and collaborators.
(72) Burkatzki, M.; Filippi, C.; Dolg, M. *J. Chem. Phys.* **2007**, *126*, 234105−234113.
(73) For the hydrogen atom, we use a more accurate BFD pseudopotential and basis set. Dolg, M.; Filippi, C., private communication.
(74) Schmidt, M. W.; Baldridge, K. K.; Boatz, J. A.; Elbert, S. T.; Gordon, M. S.; Jensen, J. H.; Koseki, S.; Matsunaga, N.; Nguyen, K. A.; Su, S.; Windus, T. L.; Dupuis, M.; J., A. M., Jr *J. Comput. Chem.* **1993**, *14*, 1347−1363.
(75) Dunning, T. H., Jr *J. Chem. Phys.* **1989**, *90*, 1007−1023.
(76) Peterson, K. A.; Woon, D. E.; Dunning, T. H., Jr *J. Chem. Phys.* **1994**, *100*, 7410−7415.
(77) Wilson, A.; van Mourik, T.; Dunning, T. H., Jr *J. Mol. Struct. (THEOCHEM)* **1997**, *388*, 339−349.
(78) Weigend, F. *Phys. Chem. Chem. Phys.* **2006**, *8*, 1057−1065.
(79) We take the diffuse functions for the heavy atoms atoms from the aug-cc-pVXZ basis sets in the EMSL Basis Set Library (http://bse.pnl.gov).
(80) Filippi, C.; Umrigar, C. J. *J. Chem. Phys.* **1996**, *105*, 213−226 As Jastrow correlation factor, we use the exponential of the sum of three fifth-order polynomials of the electron−nuclear (e-n), the electron−electron (e-e), and of pure 3-body mixed e-e and e-n distances, respectively. The Jastrow factor is adapted to deal with pseudo-atoms, and the scaling factor $\kappa$ is set to 0.6 a.u. The 2-body Jastrow factor includes five parameters in the e-e terms and four parameters for each atom type in the e-n terms. The 3-body Jastrow factor has 15 additional parameters per atom type. In both Jastrow factors, the same scaling parameter $\kappa$ is used for all inter-particle distances. For *s*-trans acrolein (3 atom types), we have therefore a total of 17 and 62 parameters in the 2-body and the 3-body Jastrow factor, respectively..
(81) Filippi, C.; Umrigar, C. J. *Phys. Rev. B* **2000**, *61*, R16291−R16294.
(82) Aquilante, F.; Barone, V.; Roos, B. *J. Chem. Phys.* **2003**, *119*, 12323−12334.
(83) Gadaczeck, I.; Krause, K.; Hintze, K. J.; Bredow, T. *J. Chem. Theory Comput.* **2012**, *8*, 986−996.
(84) Angeli, C.; Borini, S.; Ferrighi, L.; Cimiraglia, R. *J. Chem. Phys.* **2005**, *122*, 114304−114314.
(85) Angeli, C.; Borini, S.; Ferrighi, L.; Cimiraglia, R. *J. Mol. Struct. (THEOCHEM)* **2005**, *718*, 55−69.
(86) Saha, B.; Ehara, M.; Nakatsuji, H. *J. Chem. Phys.* **2006**, *125*, 014316−014330.
(87) Reguero, M.; Olivucci, M.; Bernardi, F.; Robb, M. A. *J. Am. Chem. Soc.* **1994**, *116*, 2103−2114.
(88) Losa, A. M.; Galván, I. F.; Aguilar, M. A.; Martín, M. E. *J. Phys. Chem. B* **2007**, *111*, 9864−9870.
(89) Gwaltney, S. R.; Bartlett, R. J. *J. Chem. Phys.* **1999**, *110*, 62−71.
(90) In MOLCAS, we can only perform CASSCF ground-state calculations of *s*-trans acrolein with a CAS(6,5) expansion containing the lone pair parallel to the CO bond. We cannot stabilize the expansions including the other lone pair or both lone pairs. The CASSCF energy of the $n \rightarrow \pi^*$ excited ($1^1A''$) state is instead lower if the $\sigma$ orbital corresponds to the lone pair orthogonal to the CO group. To describe the two states with the same active space and stabilize the same CAS on the ground state, we run a SA calculation without symmetry on both states and with a ratio of 995/5 in the weights for the two roots. The CASPT2 geometry optimization relaxing the first root in this fictitious SA-CASSCF calculation converges to the same geometry calculated in a single-state run with the lone pair parallel to the CO bond in the active space, regardless the choice of the basis set.
(91) We note that, for both excited states, a CAS(4,3) zero-order wave function is equivalent to a CAS(2,2) expansion only including the oxygen lone pair and the $\pi^*$ orbital, according to the Brillouin's theorem.
(92) Johnson, R. P.; Schmidt, M. W. *J. Am. Chem. Soc.* **1981**, *103*, 3244−3249.
(93) Merchán, M.; González-Luque, R.; Roos, B. O. *Theor. Chem. Acc.* **1996**, *94*, 143−154.